Journal of Applied Mechanics and Technical Physics, Vol. 40, No. 6, 1999

NUMERICAL SIMULATION OF AN OBLIQUELY INCIDENT SOLITARY WAVE

V. B. Barakhnin and G. S. Khakimzyanov

UDC 532.5: 519.6

Calculations using the finite-difference method with dynamically adaptive grids were performed within the framework of the Zheleznyak–Pelinovskii nonlinear-dispersion model and the three-dimensional potential flow model. The results are compared with calculations by other authors.

Introduction. Wiegel [1] describes the experimental investigation of Perroud [2] on the interaction of a solitary wave of amplitude a_i with a plane vertical wall on which the wave is incident at angle ψ_i. It is established that, depending on the value of ψ_i, the reflection of the wave from the wall can be regular or irregular (Mach reflection). In regular reflection, the crests of the incident and reflected waves intersect on the wall, and in Mach reflection, a third wave, called the Mach stem, appears between the wall and the point of intersection between the crests of the first two waves. Mach reflection is shown schematically in Fig. 1, where the wave crests are indicated by heavy lines.

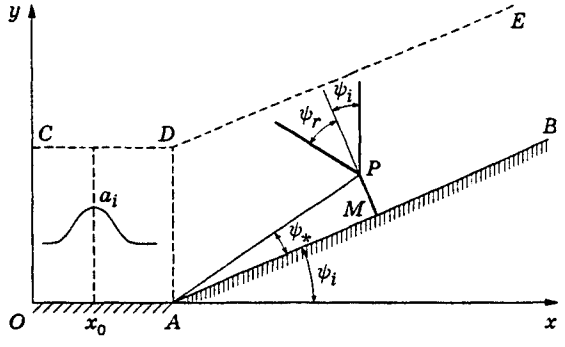

Fig. 1. Diagram of Mach reflection.

The oblique incidence of a wave on a wall was studied theoretically by Miles [3, 4]. Using a certain nonlinear-dispersion model of shallow water and assuming that the amplitude of the incident wave a_i is infinitesimal and $\psi_i^2 = O(a_i)$, he obtained analytical formulas for the maximum run-up R, the amplitude a_r of the reflected wave, the angle of reflection ψ_r, and the angle ψ_* at which the Mach stem can be seen from the point A. Of the possible schemes of interaction of the wave with the wall, he used only those wave configurations that were observed in the experiments of [2], i.e., double and triple configurations. In addition, it was assumed that away from the interaction zone, all waves have the shape of solitons and, in the case of Mach reflection, the parameters of the waves satisfy additional conditions of resonance interaction. Under these assumptions, the following formula for the maximum run-up was obtained:

Institute of Computational Technologies, Siberian Division, Russian Academy of Sciences, Novosibirsk 630090. Translated from Prikladnaya Mekhanika i Tekhnicheskaya Fizika, Vol. 40, No. 6, pp. 17–25, November–December, 1999. Original article submitted June 27, 1997; revision submitted April 1, 1998.

 0021-8944/99/4006-1008 $22.00

$$\frac{R}{a_i} = \begin{cases} \dfrac{4}{1+(1-3a_i/\psi_i^2)^{1/2}} & \text{for} \quad \dfrac{\psi_i^2}{3a_i} \geqslant 1, \\ \left(1+\dfrac{\psi_i}{(3a_i)^{1/2}}\right)^2 & \text{for} \quad \dfrac{\psi_i^2}{3a_i} \leqslant 1. \end{cases} \tag{1}$$

Thus, if a solitary wave is incident on the wall at an angle, the maximum run-up can reach a value $R_* = 4a_i$.

A serious disadvantage of the work of [2] is that the laboratory experiments were carried out in a rather shallow tank with a water layer 4 cm deep. As is pointed out in [5], the shape of a wave propagating in such a thin layer changes considerably because of capillary and viscous effects, so that the wave interacting with the wall has a shape different from that prescribed at the initial time. In the experiments of Melville [5], the tank was 30 cm in depth, but the values obtained for R did not exceed $2a_i$. Serebrennikova and Frank [6] proved that such small values of the run-up are explained by the fact that Melville [5] studied only the initial stage of interaction of a wave with a wall, whereas stationary values of R are obtained only when the wave travels a distance that is at least one order of magnitude larger than that in the of experiments Melville. This implies that the horizontal dimensions of the tank must be tens of times larger (Melville used a tank with dimensions of 18.3×6.2 m). Since creating such experimental installations is problematic at present, numerical simulations are of great significance in studies of the oblique incidence of solitary waves.

A numerical simulation of oblique incidence is described, for example, in [7] for $a_i/h_0 = 0.05$, where h_0 is the depth of the tank (below, we set $h_0 \equiv 1$). The mathematical model from which Miles obtained the theoretical predictions was used in this calculation. It turned out that the values of ψ_* and ψ_r are in agreement with theoretical values, but for a_r and, especially, for the maximum run-up R, the disagreement with the theory is marked. Miles's theory is probably applicable for $a_i \ll 0.05$ and small values of ψ_i. At the same time, it is known [6–9] that as the values of a_i and ψ_i decrease the time of attainment of a quasistationary regime of interaction increases rapidly. If we take into account that with decrease in a_i, the length of a solitary wave and, hence, the number of grid points necessary for a good description of the wave increase, it becomes clear that at present it is hardly possible to determine the upper bounds (for the parameters a_i and ψ_i) of applicability of Miles's theory by numerical simulations. Funakoshi [7] points out that even for $a_i = 0.05$, some calculations were impossible to finish because of high expenditure of computer resources.

At the same time, the incidence of waves of finite rather than infinitesimal amplitude is of practical interest. In the absence of both reliable experimental data and a theory for the oblique incidence of finite-amplitude waves, numerical simulation is the only method for studying this process. Funakoshi used the finite-difference method of calculation for a wave with an amplitude $a_i = 0.05$. Tanaka [9] employed the spectral method for $a_i = 0.3$. O. A. Serebrennikova and A. M. Frank performed a series of calculations for $a_i = 0.05$–0.30 within the framework of the discrete model of an incompressible fluid. Since there are differences in numerical results for some values of the parameters, calculations should be carried out on the basis of different mathematical models and algorithms.

The present paper reports results of calculations performed by the finite-difference method with dynamically adaptive grids within the framework of the Zheleznyak–Pelinovskii nonlinear-dispersion model and the three-dimensional potential flow model. The results are compared with calculations by other authors.

1. Method of Solution. First of all, we note that all data are given in dimensionless variables. Spatial variables are made dimensionless by division by h_0 and the time was multiplied by $\sqrt{g/h_0}$, where g is the acceleration of gravity.

The flow domain is shown in Fig, 1. At $t = 0$, the crest line of the solitary wave is parallel to the Oy axis, and the crest has abscissa x_0; in calculations using the nonlinear-dispersion model, the point x_0 is chosen to the right of the interval AD, and it is chosen to the left of this integral for the potential flow model.

For the nonlinear-dispersion model, the solitary wave at the initial time is given by the formulas

$$\eta(x,y,0) = a_i \operatorname{sech}^2 X, \qquad X = \sqrt{3a_i/(4(a_i+1))}(x-x_0); \tag{2}$$

$$u(x,y,0) = U_0\eta/(1+\eta), \qquad v(x,y,0) = 0,$$

where $U_0 = \sqrt{1 + a_i}$. For the potential flow model, we use Ovsyannikov's formulas [10] which, after elementary transformations, become

$$\eta(x, y, 0) = a_i \operatorname{sech}^2 X,$$

$$u(x, y, z, 0) = U_0 \frac{\eta}{\eta + 1} - \frac{a_i^2}{U_0}\left[\frac{1}{4} - \frac{3}{4}\left(\frac{z+1}{\eta+1}\right)^2\right]\left[2\frac{\eta - 1}{\eta + 1}\operatorname{sech}^2 X + \frac{3 - \eta}{\eta + 1}\operatorname{sech}^4 X\right],$$

$$v(x, y, z, 0) = 0, \quad w(x, y, z, 0) = \sqrt{3a_i^3}\,(1 + z)\cosh X \sinh X/(a_i + \cosh^2 X)^2.$$

In these equations, η is the elevation of the free surface, and u, v, and w are the velocity components.

Numerical implementation of the Zheleznyak–Pelinovskii nonlinear-dispersion model [11] is complicated by the presence in the equations of mixed higher-order derivatives with respect to time and spatial variables. The order of these derivatives can be reduced by introducing new dependent variables in such a way as to split the original system of equations into an elliptic equation and an inhomogeneous hyperbolic system [12]. For numerical calculation of the split system, we use an explicit finite-difference predictor–corrector scheme with automatically adjustable approximation viscosity [13]. We use the approximation of the nondivergent part of the hyperbolic system at the predictor step of the scheme and the approximation of the divergent part at the corrector step. Before both steps of the predictor-corrector scheme, the elliptic equation is solved by a 9-point scheme of the "oblique cross" type [14] with a self-adjoint positive definite operator, obtained by the integrointerpolation method of [12].

The calculation algorithm for three-dimensional potential flows of an ideal fluid with a free boundary is described in [15]. At each time step, the values of the potential φ at the free-surface grid points are first determined. Then, the Laplace equation written in a moving curvilinear coordinate system is solved by the iterative method of successive over-relaxation, and values of the potential are determined at the grid points in the interior of the domain and on the fixed rigid boundaries. A new position of the free surface η is obtained from the kinematic condition, and an adaptive grid is constructed for t_{n+1}. At each time step, the cycle of calculations is repeated several times until the quantities φ and η are computed with specified accuracy.

In numerical calculations of the problem, we used curvilinear grids that were adaptable to the shape of the domain and depended on the solution. These grids have certain advantages in comparison with uniform grids because of simpler realization of the boundary conditions. In addition to this, owing to the adaptation of the grid to the solution, high accuracy is attained for a small number of grid points by increasing their concentration in the regions of singularities of the phenomenon studied: in the neighborhood of the crests of the incident and reflected waves, the Mach stem, and the region of run-up.

When curvilinear grids are used, the moving domain $\Omega(t)$ occupied by the fluid at each time t is mapped onto a fixed calculation domain Q which is a unit square or a unit cube, depending on the dimension of the problem. This mapping is performed on the basis of the on-to-one nondegenerate transformation of the coordinates. The equations and initial and boundary conditions are written in a new coordinate system [12, 15].

In calculations using the two-dimensional nonlinear-dispersion model, the grid is constructed as follows [16]. In the direction of wave propagation, the grid points are concentrated by the one-dimensional equidistribution method, which takes into account the position of the grid points at the previous time step, and the controlling function is chosen so that the maximum concentration of the grid is achieved in the regions of maximum elevation of the free surface η. Along the second direction, the grid points are arranged according to the law of geometric progression, concentrating at the wall OAB (see Fig. 1).

For three-dimensional problems, the grid is constructed by a combined method whose main idea is that the one-dimensional equidistribution method is used for each coordinate direction. Along the first and second coordinate directions, the concentration of the grid points depends on η, and along the straight coordinate lines issuing from the bottom grid points and intersecting the free surface, the grid point concentration depends on the absolute value of the velocity.

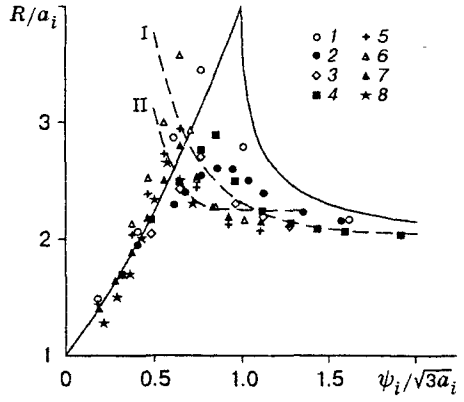

Fig. 2. Dependence of R/a_i on $\psi_i/\sqrt{3a_i}$: the points are calculation results; the solid curve refers to the theoretical dependence (1) and the dashed curves refer to the theoretical dependence (3) for $a_i = 0.1$ (I) and 0.5 (II); for $a_i = 0.05$, points 1 refer to data of [7] and 2 to the PFM, for $a_i = 0.1$, points 3 and 4 refer to the NLDM and PFM, respectively, for $a_i = 0.3$, points 5 and 6 refer to the data of [9] and [6], respectively, and points 7 refer to the PFM, and for $a_i = 0.5$, points 8 refer to the PFM.

The above algorithm of constructing three-dimensional adaptive grids allows one to obtain only slight changes in the amplitude and shape of the incident wave even when it travels distances of about 30 its length. Note that in [8], where the grids were adapted only to the boundaries of the domain, the amplitude of the wave decreased by 10% at the corresponding time.

The boundary conditions were specified as follows. The artificial boundary CDE (see Fig. 1) was placed away from the wall OAB [at distances of 40–70 for the nonlinear-dispersion model (NLDM) and 80 for the potential flow model (PFM)], and as a result, the boundary did not affect the interaction between the incident wave and the wall for a long time. Therefore, the partial derivatives of the required function with respect to y were set equal to zero on the artificial boundary. On the rigid wall OAB, the condition of no normal flow was used.

Calculation were performed in a moving calculation domain attached to the crest of the incident wave. A similar technique was used, e.g., in [6, 7]. The conditions of unperturbed flow were used on the right side of the calculation domain. On the left side, we usually imposed the condition of no normal flow, which did not change the flow pattern markedly since the waves generated by this condition did not penetrate into the calculation domain. However, in calculations using the potential flow model, for angles $\psi_i \geqslant 40°$ on the left boundary it is appropriate to use extrapolation along the crest of the reflected wave.

In calculations using the nonlinear-dispersion model, the dimension of the calculation domain along the Ox axis was 62.5 and the number of grid points was 251×21. For the three-dimensional potential flow model, the dimension of the calculation domain ranged from 40 to 30 (decreased with increase of a_i) and the number of grid points was varied from $121 \times 81 \times 8$ to $121 \times 81 \times 12$. For verification of convergence, some calculations were carried out with a $241 \times 161 \times 16$ grid.

2. Results of Numerical Simulation. Figure 2 shows the run-up R_i/a_i versus the quantity $\psi_i/\sqrt{3a_i}$ for various amplitudes of the incident wave. Evidently, for each a_i, this dependence is not monotonic. For small ψ_i, the value of R/a_i is close to unity. Then, with increase in ψ_i, the relative run-up also increases. For a certain critical $\psi_{i,*}$, the run-up reaches a maximum value, and with a further increase in ψ_i, it decreases monotonically. Similar qualitative behavior of the dependence of R/a_i on $\psi_i/\sqrt{3a_i}$ was obtained in [6, 7, 9]. Quantitative comparison gives satisfactory agreement between calculations using the potential flow model and the results of [9] for $a_i = 0.3$. A large difference between our results and the calculations of [6, 7] is observed in the neighborhood of the critical angles of incidence $\psi_{i,*}$. The discrepancy of the results decreases

with distance from this point.

Theoretical curves of (1) are shown in Fig. 2. One can see that for finite values of the amplitude a_i (even for $a_i = 0.5$) the calculation results are near the solid curve of (1) (see the second equation) for Mach reflection, although this curve was obtained for the run-up of waves of infinitesimal amplitude. At the same time, in our calculations and in the calculations of [6, 7, 9], the values of R/a_i differ markedly from dependence (1) (see the first equation) for regular reflection. The calculation data are shifted to the left from curve of (1) (see the first equation). The maximum of the quantity R/a_i is also shifted to the left from the point $\psi_i/\sqrt{3a_i} = 1$, and the shift becomes larger with increase in a_i. In contrast, in calculations for $a_i = 0.05$ using the potential flow model, the maximum is attained at $\psi_i/\sqrt{3a_i} \approx 1$.

We also note that in our calculations, in contrast to the calculations of [6, 7] and the theory of [4], the quantity R/a_i behaves rather smoothly when ψ_i is changed. This is especially evident for $a_i = 0.05$.

Miles [3] obtained one more formula for the run-up of a wave of infinitesimal amplitude with regular reflection:

$$\frac{R}{a_i} = 2 + a_i\Big(\frac{3}{2\sin^2\psi_i} - 3 + 2\sin^2\psi_i\Big). \tag{3}$$

This formula is derived without the assumption that ψ_i is small, i.e., for $\psi_i \gg a_i$. M. Tanaka compared the values he obtained for the maximum run-up in regular reflection with the values of the run-up calculated from Eq. (3) and obtained qualitative agreement, although the condition $\psi_i \gg a_i$ was violated in the calculations. Two curves of (3) for $a_i = 0.1$ and $a_i = 0.5$ are shown in Fig. 2. One can see that in the case of $a_i = 0.1$, the calculated run-up for the NLDM agrees with formula (3) for $\psi_i > \psi_{i,*}$. For the indicated amplitude, the PFM yields calculated values that agree with (3) for $\psi_i/\sqrt{3a_i} > 1$.

In the interval $a_i = 0.1$–0.2, the point of intersection of curve (3) and the Mach reflection curve (1) (see the second equation) differs only slightly from the point corresponding to the maximum run-up in calculations using the NLDM. For amplitudes $a_i \geqslant 0.3$, calculations of regular reflection using the PFM agree with formula (3), and, as for the NLDM, the calculation data agree with dependence (1) (see the second equation) in the region of Mach reflection.

Another important characteristic of the process considered is the amplitude of the reflected wave a_r. To calculate this amplitude, we used the following approach. First, on every coordinate curve of the second family, we found the grid point at which the elevation of the reflected wave is maximum. These grid points were then used to draw, by the least squares method, a line that was identified with the crest of the reflected wave. The left and right parts of the crest adjacent to the left boundary of the calculation domain and the region of joining of the reflected and incident waves (the point P in Fig. 1) were eliminated from the subsequent analysis; the change in elevation along the entire remaining part of the crest did not exceed 3%. Finally, as a_r we used the arithmetic mean of η at the grid points in this part of the crest.

Figure 3 shows the dependence of a_r/a_i on $\psi_i/\sqrt{3a_i}$. One can see that our results and the calculation results obtained in [6, 7, 9] are in qualitative agreement with Miles's theory, according to which

$$\frac{a_r}{a_i} = \begin{cases} 1 & \text{for} \quad \psi_i^2/(3a_i) \geqslant 1, \\ \psi_i^2/(3a_i) & \text{for} \quad \psi_i^2/(3a_i) \leqslant 1. \end{cases} \tag{4}$$

As noted in [6], calculations agree with the quadratic dependence (4) in the case of Mach reflection. For $a_i = 0.05$, results of calculations using the PFM coincide with theoretical data both qualitatively and quantitatively. For larger values of a_i, the calculated curves are shifted to the left from the theoretical curve and are steeper than the latter.

Curves of the angles of reflection are shown in Fig. 4. The angle ψ_r is defined as the angle between the normal to the wall and the rectilinear crest of the reflected wave and is determined by the procedure described above. One can see that for $a_i = 0.05$, the calculated data are in good agreement with the results of Funakoshi and with Miles's theory. With increase in the amplitude of the incident wave, the disagreement with the values calculated from the theoretical formula

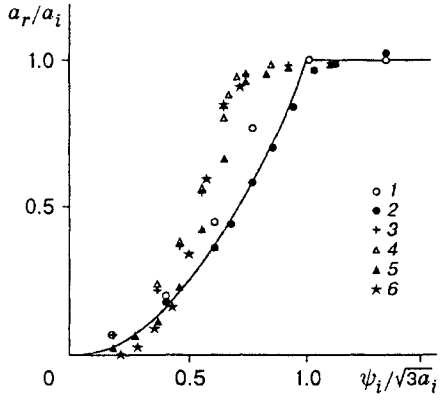

Fig. 3

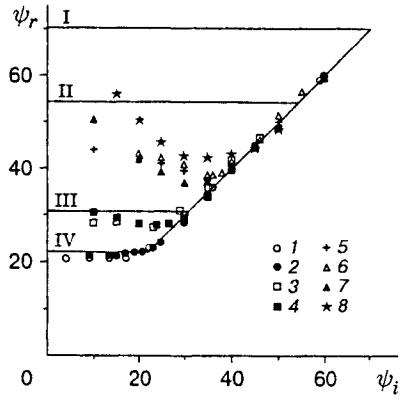

Fig. 4

Fig. 3. a_r/a_i versus $\psi_i/\sqrt{3a_i}$: the points are calculation results; the solid curve refers to the theoretical formulas of Miles [3, 4]; for $a_i = 0.05$, points 1 refer to data of [7] and points 2 refer to the PFM, for $a_i = 0.3$, points 3 and 4 refer to the data of [9] and [6], respectively, and point 5 refer to the PFM, and for $a_i = 0.5$, points 6 refer to the PFM.

Fig. 4. ψ_r versus ψ_i: the points are calculation results; the solid curve refers to the theoretical formulas of Miles [3, 4] for $a_i = 0.5$ (I), 0.3 (II), 0.1 (III), and 0.05 (IV); for $a_i = 0.05$, points 1 refer to the data of [7] and points 2 refer to the PFM, for $a_i = 0.1$, points 3 refer to the data of [6] and points 4 refer to the PFM, for $a_i = 0.3$, points 5 and 6 refer to the data of [9] and [6], respectively, and points 7 refer to the PFM, and for $a_i = 0.5$, points 8 refer to the PFM.

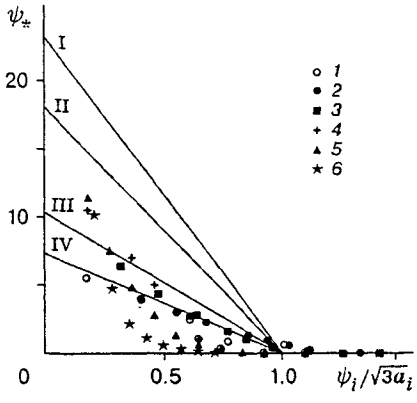

Fig. 5

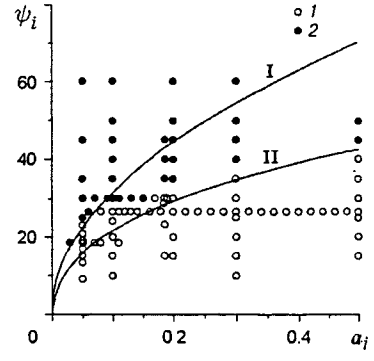

Fig. 6

Fig. 5. Dependence of ψ_* on $\psi_i/\sqrt{3a_i}$: the points are calculation results; the solid curves refer to the theoretical formulas of Miles [3, 4] for $a_i = 0.5$ (I), 0.3 (II), 0.1 (III), and 0.05 (IV); for $a_i = 0.05$, points 1 refer to the data of [7] and points 2 refer to the PFM, for $a_i = 0.1$, points 3 refer to the PFM, for $a_i = 0.3$, points 4 refer to the data of [9] and points 5 refer to the PFM, and for $a_i = 0.5$, points 6 refer to the PFM.

Fig. 6. The type of reflection for various values of a_i and ψ_i: curves I and II refer to relations $\psi_i = \sqrt{3a_i}$ and (6), respectively; points 1 and 2 refer to Mach and regular reflections, respectively.

$$\psi_r = \begin{cases} \psi_i & \text{for } \psi_i^2/(3a_i) \geqslant 1, \\ (3a_i)^{1/2} & \text{for } \psi_i^2/(3a_i) \leqslant 1 \end{cases}$$

becomes more marked; at the same time, there is agreement with the calculations of [6, 9] (except for the angle $\psi_i = 10°$). We also note that in the calculations for the potential flow model, the curves have a larger deflection than in calculations by other authors. It is interesting that even for a very large amplitude $a_i = 0.5$, the qualitative character of the dependence remains the same as for $a_i = 0.2$ and $a_i = 0.3$. In addition, with

decrease in ψ_i, the values of ψ_r approach the theoretical value $\sqrt{3a_i}$.

Figure 5 shows the angle ψ_* (see Fig. 1) versus $\psi_i/\sqrt{3a_i}$. For $a_i = 0.05$, the numerical results obtained herein and by Funakoshi agree again with the theoretical formula

$$\psi_* = \begin{cases} 0 & \text{for} \quad \psi_i^2/(3a_i) \geqslant 1, \\ (a_i/3)^{1/2}(1 - \psi_i/(3a_i)^{1/2}) & \text{for} \quad \psi_i^2/(3a_i) \leqslant 1. \end{cases} \tag{5}$$

However, with increase in the amplitude of the incident wave, the values of ψ_* obtained by the potential flow model deviate more and more from formula (5). And the difference is not only qualitative but also quantitative. The curve of (5) for Mach reflection is a line segment whereas calculations yielded more complicated power-law dependences.

Finally, using the results of calculations for the potential flow model, we determine the dependence of the type of reflection on the values of a_i and ψ_i. In the present work, the type of reflection is determined from the angle ψ_*. If by the moment $t = 300$, the condition $\psi_* < 0.5°$ is satisfied and ψ_* does not grow further, then the reflection is considered regular. Figure 6 shows the dependence of the reflection type on ψ_i and a_i. One can see that for small amplitudes of the incident wave ($a_i < 0.08$), the value of ψ_i^0 that distinguishes Mach reflection from regular reflection agrees with Miles's formula $\psi_i = \sqrt{3a_i}$. Further, with increase in a_i, the quantity ψ_i^0 becomes smaller than $\sqrt{3a_i}$. For $a_i > 0.3$, the value of ψ_i^0 is determined with sufficient accuracy from the condition of the equality of expressions (1) (see the second equation) and (3), i.e., ψ_i^0 is close to the root ψ of the equation

$$\Big(1 + \frac{\psi}{\sqrt{3a_i}}\Big)^2 - 2 - a_i\Big(\frac{3}{2\sin^2\psi} - 3 + 2\sin^2\psi\Big) = 0. \tag{6}$$

Comparison of the calculation results obtained by different authors shows that all results are in qualitative agreement and considerable quantitative differences are obtained only for the run-up at the wall. For $a_i = 0.05$, the values of ψ_r, a_r, and ψ_* calculated using the potential flow model are consistent with the theoretical predictions of Miles. For $a_i > 0.1$, there is considerable disagreement with the theory. However, up to $a_i = 0.3$, the calculations yields the same configuration of interacting waves as in Miles's theory. Moreover, in our calculations, as in Miles's theory, the cross section of a reflected wave with $a_i \leqslant 0.2$ has the shape of a soliton, or, in other words, the neighborhood of its crest is described by expression (2) if in the latter one replaces a_i by the calculated value of a_r, sets $x_0 = 0$, and uses, instead of x, the distance from the crest of the reflected wave in the perpendicular direction.

At the same time, for $a_i > 0.3$, a different scheme of interaction between the wave and the wall was observed in the calculations using the potential flow model. For example, for $a_i = 0.5$, in the case of Mach reflection there are two reflected waves, and the crest of the Mach stem has no part with constant elevation (in contrast to the case $a_i \leqslant 0.3$), decreasing just from the wall. It is interesting that for $a_i = 0.5$, the cross sections of the Mach stem have the shape of two-dimensional solitary waves (2). In this case, in a certain range of values of ψ_i, the amplitude of these waves is larger than the critical amplitude of a solitary wave, which is about 0.83. For example, for $a_i = 0.5$ and $\psi_i = 40°$, after attainment of stationarity, the free-surface profile along the wall AB (see Fig. 1) has the shape of a solitary wave with oscillations behind the crest and a maximum elevation of 1.32 at the point M. We emphasize that the wave at the wall with this supercritical value of the amplitude propagates without breaking. The stability of this wave can probably be explained by the fact that for $a_i = 0.5$ the flow pattern in the Mach stem is complex with velocities having nonzero component along the crest.

This work was performed within the framework of the project No. 43 (Siberian Division, Russian Academy of Sciences) and supported by the Russian Foundation for Fundamental Research (Grant No. 97-01-00819).

REFERENCES

1. R. L. Wiegel, *Oceanographical Engineering*, Prentice-Hall, Englewood Cliffs, NJ (1964).
2. P. H. Perroud, "The solitary wave reflection along a straight vertical wall at oblique incidence," PhD Thesis, Univ. Calif., Berkeley (1957).
3. J. M. Miles, "Obliquely interacting solitary waves," *J. Fluid Mech.*, **79**, 157–169 (1977).
4. J. M. Miles, "Resonantly interacting solitary waves," *ibid.*, pp. 171–179.
5. W. K. Melville, "On the Mach reflection of a solitary wave," *J. Fluid Mech.*, **98**, 285–297 (1980).
6. O. A. Serebrennikova and A. M. Frank, "Numerical simulation of Mach reflection for solitary waves," *Prikl. Mekh. Tekh. Fiz.*, No. 5, 15–24 (1993).
7. M. Funakoshi, "Reflection of obliquely incident solitary waves," *J. Phys. Soc. Jpn.*, **49**, No. 6, 2371–2379 (1980).
8. G. S. Khakimzyanov, "On the numerical simulation of three-dimensional fluid flows with surface waves using adaptive grids," in: *Proc. All-Union Colloquium on Methods and Problems of Wave Hydrodynamics* (Rostov-on-Don, September 23–27, 1990), Krasnoyarsk (1990), pp. 103–108.
9. M. Tanaka, "Mach reflection of a large-amplitude solitary wave," *J. Fluid Mech.*, **248**, 637–661 (1993).
10. L. V. Ovsyannikov, "The parameters of cnoidal waves," in: *Problems of Mathematics and Mechanics* [in Russian], Nauka, Novosibirsk (1983), pp. 150–166.
11. M. I. Zheleznyak and E. N. Pelinovskii, "Physicomathematical models for the incidence of tsunami on a shore," in: *Incidence of Tsunami on Shore* [in Russian], Inst. of Appl. Phys., Gor'kii (1985), pp. 8–33.
12. V. B. Barakhnin and G. S. Khakimzyanov, "On the algorithm of numerical solution for the equations of a nonlinear-dispersion model of shallow water," *Vychisl. Tekhnol.*, **1**, No. 3, 5–20 (1996).
13. V. B. Barakhnin and G. S. Khakimzyanov, "Adaptive-grid numerical solution of one-dimensional amd two-dimensional problems for the shallow-water equations," in: *Adv. Math.: Comput. and Appl.*, Proc. of the AMCA–95, NCC Publisher, Novosibirsk (1995), pp. 144–153.
14. A. A. Samarskii and V. B. Andreev, *Finite-Difference Methods for Elliptic Equations* [in Russian], Nauka, Moscow (1976).
15. Yu. I. Shokin and G. S. Khakimzyanov, "Finite-difference method for calculating three-dimensional potential flows with a free boundary," *Vychisl. Tekhnol.*, **1**, No. 1, 154–176 (1992).
16. V. B. Barakhnin and G. S. Khakimzyanov, "Application of dynamically adaptive grids in the problems of shallow-water theory," *Vopr. Atom. Nauki Tekh., Ser. Mat. Model. Fiz. Prots.*, **2**, 36–44 (1997).